Original Investigation

Lepidic Predominant Pulmonary Lesions (LPL): CT-based Distinction From More Invasive Adenocarcinomas Using 3D Volumetric Density and First-order CT Texture Analysis

Jeffrey B. Alpert, MD, Henry Rusinek, PhD, Jane P. Ko, MD, Bari Dane, MD, Harvey I. Pass, MD, Bernard K. Crawford, MD, Amy Rapkiewicz, MD, David P. Naidich, MD

Rationale and Objectives: This study aimed to differentiate pathologically defined lepidic predominant lesions (LPL) from more invasive adenocarcinomas (INV) using three-dimensional (3D) volumetric density and first-order texture histogram analysis of surgically excised stage 1 lung adenocarcinomas.

Materials and Methods: This retrospective study was institutional review board approved and Health Insurance Portability and Accountability Act compliant. Sixty-four cases of pathologically proven stage 1 lung adenocarcinoma surgically resected between September 2006 and October 2015, including LPL ($n = 43$) and INV ($n = 21$), were evaluated using high-resolution computed tomography. Quantitative measurements included nodule volume, percent solid volume (% solid), and first-order texture histogram analysis including skewness, kurtosis, entropy, and mean nodule attenuation within each histogram quartile. Binomial logistic regression models were used to identify the best set of parameters distinguishing LPL from INV.

Results: Univariate analysis of 3D volumetric density and histogram features was statistically significant between LPL and INV groups ($P < .05$). Accuracy of a binomial logistic model to discriminate LPL from INV based on size and % solid was 85.9%. With optimized probability cutoff, the model achieves 81% sensitivity, 76.7% specificity, and area under the receiver operating characteristic curve of 0.897 (95% confidence interval, 0.821–0.973). An additional model based on size and mean nodule attenuation of the third quartile (Hu_Q3) of the histogram achieved similar accuracy of 81.3% and area under the receiver operating characteristic curve of 0.877 (95% confidence interval, 0.790–0.964).

Conclusions: Both 3D volumetric density and first-order texture analysis of stage 1 lung adenocarcinoma allow differentiation of LPL from more invasive adenocarcinoma with overall accuracy of 85.9%–81.3%, based on multivariate analyses of either size and % solid or size and Hu_Q3, respectively.

Key Words: Lepidic predominant; invasive adenocarcinoma; volumetric density; histogram.

INTRODUCTION

To date, numerous publications have correlated the pathologic spectrum of lung adenocarcinoma with computed tomography (CT) findings (1–7). Although differentiation among these varying CT patterns has important management implications, morphologic distinctions along the spectrum of peripheral adenocarcinomas have shown considerable overlap, including pronounced inter- and intraobserver variability in visual differentiation of nodule features, rendering sole reliance on morphologic characterization problematic (5,7–10). Based on these limitations, recent efforts have moved

Acad Radiol 2017; ■:■■–■■

From the Department of Radiology, New York University Langone Medical Center, 660 First Avenue, 3rd Floor, New York, NY 10016 (J.B.A., H.R., J.P.K., B.D., D.P.N.); Department of Cardiothoracic Surgery (H.I.P., B.K.C.); Department of Pathology, New York University Langone Medical Center, New York, New York (A.R.). Received May 19, 2017; revised July 11, 2017; accepted July 12, 2017. No grant support was provided for this work. There is no conflict of interest to report. **Address correspondence to:** J.B.A. e-mail: jeffrey.alpert@nyumc.org

http://dx.doi.org/10.1016/j.acra.2017.07.008

toward quantitative CT methods of differentiating pathologic subtypes, specifically documenting a role for advanced, quantitative assessment of peripheral lung nodules, while taking into account previous evidence that nodule size positively correlates with tumor invasiveness (11,12). Most recently, quantitative CT assessment has included both two-dimensional and three-dimensional (3D) volumetric density and texture or histogram analysis to more precisely characterize these lesions. Encouraging preliminary results were obtained using a 3D volumetric model that emphasizes the proportion of solid component(s) of part-solid lung nodules to differentiate between three specimen groups: a combined group of preinvasive adenocarcinoma in situ (AIS) and minimally invasive adenocarcinoma (MIA), lepidic predominant adenocarcinoma (LPA), and more invasive forms of adenocarcinoma (INV); a statistically significant difference in percentage solid volume (% solid) was found between LPA and INV groups (13).

As defined by the International Association for the Study of Lung Cancer (IASLC) and the World Health Organization, LPA is a variant of invasive adenocarcinoma in which bland, non-malignant cells predominate, associated with at least one focus of invasion measuring >5 mm in largest dimension, with evidence of tumor necrosis, invasion of lymphatics, blood vessels or pleura, or spread through alveolar spaces (14). In distinction, more invasive subtypes include acinar, papillary, and micropapillary predominant subtypes, as well as the solid tumor subtype. Pathologic subtypes of lepidic predominant and more invasive lesions have shown to have clear prognostic implications (15–19). In a study of 210 postsurgical patients, a combined group of patients with AIS, MIA, and LPA had a 5-year survival of 93%, whereas patients with more invasive subtypes had a worse prognosis, with 71%, 68%, 39%, and 38% 5-year survivals for papillary, acinar, solid, and micropapillary-predominant types, respectively ($P < .0001$) (19). More specifically, patients with AIS and MIA have been reported to have 5-year disease-free survival (DFS) near 100% following surgical resection, with non-mucinous LPA having DFS of 90%–94% (15,19–21). Furthermore, the cumulative incidence of recurrence was zero among patients with AIS and MIA, and disease in patients with LPA was significantly less likely to recur versus more invasive forms of adenocarcinoma (5-year cumulative incidence of recurrence of 8% vs 19%, $P = .003$) (15).

In addition to increasing emphasis on volumetric assessment of peripheral lung nodules, there has also been a corresponding, if less extensive, interest in use of advanced texture analysis as an additional or alternative quantitative measurement tool. This includes quantitative histogram analysis, which uses attenuation values of each voxel and their distribution throughout the lung nodule to provide tissue characterization and lesion differentiation (22–29).

When considering the clinical implications between lepidic predominant lesions (LPL) and INV subtypes, and the current ability to differentiate these subtypes using quantitative imaging features, the aims of the present study include (1) reassessment of prior 3D volumetric density results after inclusion of a larger number of pathologically documented MIA; (2) assessment of the utility of first-order texture histogram measures of nodule attenuation, given that histogram analysis does not entail a fixed density threshold to separate solid from subsolid nodule components; and (3) reinterpretation of these results in light of the original IASLC/American Thoracic Society (ATS)/European Respiratory Society (ERS) classification with a proposal to combine the three lepidic predominant subtypes of peripheral lung adenocarcinoma (AIS, MIA, and LPA) as a single clinical group of LPL, distinct from the remaining INV subtypes. The rationale for such a grouping is the knowledge of much longer DFS in LPL patients (15,17–20).

MATERIALS AND METHODS

Patient and CT Data

This retrospective study was compliant with the Health Insurance Portability and Accountability Act and was approved by the institutional review board; informed consent was waived. Twenty-six surgically resected MIA specimens were added to a previously reported preexisting group of 38 pathologically proven, surgically resected stage 1 lung adenocarcinomas (11). This article differs from the prior effort by reinterpreting a larger data set, with the intention of assessing the ability of advanced CT techniques to differentiate between a group of combined lepidic predominant lesions and a group of more invasive adenocarcinoma subtypes. For this purpose, analysis has been expanded to include first-order texture analysis of lung adenocarcinoma subtypes, in addition to several 3D volumetric density measurements.

All surgically resected pathologically confirmed stage 1 adenocarcinomas in this study were consecutively identified at our institution between September 19, 2006 and October 21, 2015 via search of a thoracic surgical and pathology database. The timing of surgical excision was determined by thoracic surgeons, frequently in consensus in a multidisciplinary group of pulmonary specialists including pulmonologists, oncologists, pathologists, nuclear medicine specialists, and radiologists. MIA specimens were diagnosed in concordance by two pulmonary pathologists at different time points, unaware of CT findings using the IASLC/ATS/ERS international multidisciplinary classification (14).

Only noncontrast CT studies including thin-section (≤1.5 mm) axial images performed within 90 days of surgery were included. Fifty-three potential subjects were excluded because of the presence of IV contrast, the absence of thin-section axial CT images, or a time interval between CT and surgery more than 90 days. However, a total of 64 appropriate cases were obtained from 62 patients (45 women and 17 men, mean age 70.4 years, range 47–84); two patients each had two MIA specimens. Specimens were classified as 31 MIA and 12 LPA, comprising a group of 43 LPL, as well as 21 INV.

All chest CT examinations were performed on multidetector CT scanners with either 64- or 128-detector row configuration

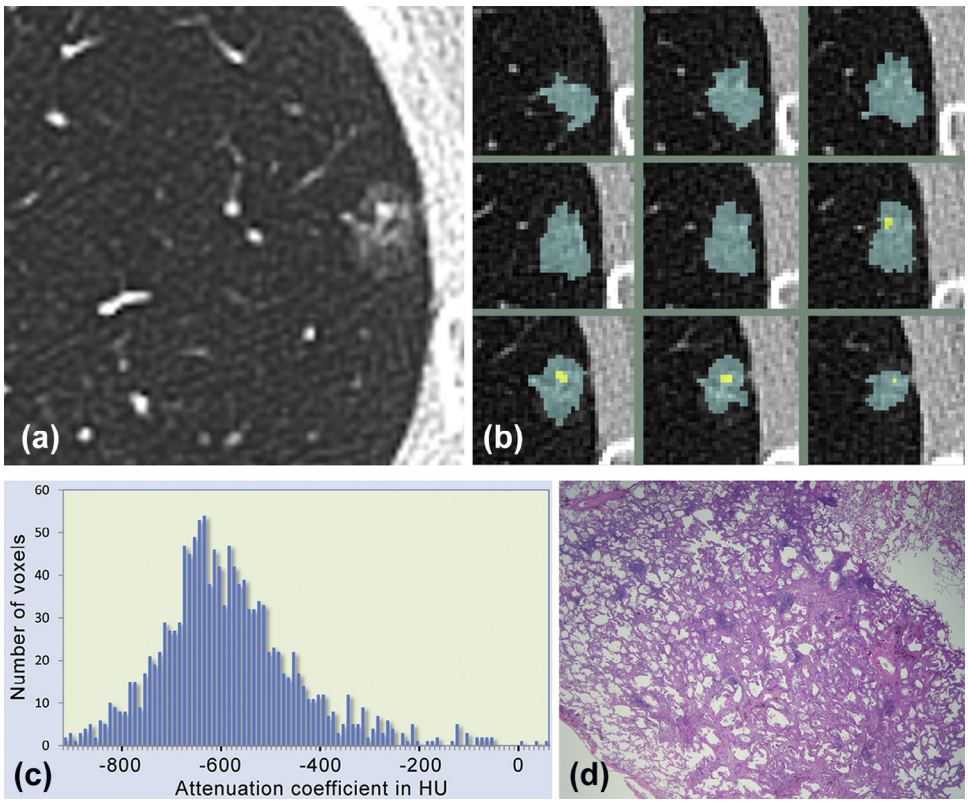

Figure 1. Quantitative computed tomography (CT), histogram, and histologic evaluation of minimally invasive adenocarcinoma (MIA) in a 68-year-old woman. **(a)** Thin-section (1 mm) noncontrast axial CT image of the part-solid lesion, which measures 1.2 by 0.9 cm and visibly demonstrates a discrete 2-mm solid component. **(b)** Automated nodule segmentation with volume of interest (VOI) masks overlying the total nodule (*blue*) and the solid portion (*yellow*) of the nodule. **(c)** Corresponding histogram analysis, which examines the number of voxels at each attenuation measurement. **(d)** Histology demonstrating lepidic thickening of normal lung architecture as well as areas of invasion (*center*) with scattered lymphoid aggregates (hematoxylin-eosin stain; original magnification, ×20). (Color version of figure is available online.)

(Definition AS+ or Definition Flash; Siemens, Malvern, PA). Although chest CT imaging protocol varied in this retrospective study, all noncontrast examinations were performed with contiguous 1-mm axial sections reconstructed at 0.8-mm intervals. Imaging parameters also included 50–160 mAs tube current times, 120 kVp, gantry rotation times of 0.33–0.5 seconds, and variable tube current modulation. Data were reconstructed with a high-frequency kernel and initially viewed in lung window. Data were anonymized before analysis.

Automated 3D Nodule Segmentation, Volumetric Density, and First-order Texture Analysis

Nodule size was determined by the average of the maximum perpendicular measurements on the axial CT image on which the nodule was the largest. Each nodule was then segmented on CT data using a previously reported locally developed investigational method (30). MIA nodules were segmented by a thoracic radiologist with 7 years of post-fellowship experience and a senior radiology resident, who were aware of pathologic diagnoses. After a training session, observers individually placed over-inclusive volumes of interest (VOIs) around subsolid nodules on every 1-mm CT image on which the nodule was visualized (Fig 1). The VOI encompassed the nodule and included a rim of 1–3 mm of surrounding lung. Observers manually excluded intervening blood vessels or chest wall structures within or abutting the nodule margin. VOI delineation took 35 seconds on average. As previously documented, this segmentation technique has excellent interobserver variability with interclass correlation coefficient ranging from 0.987 to 0.996 (13,30). Each of the additional cases of MIA was then added to the preexisting group of MIA, LPA, and INV specimen nodules (13). The program then automatically normalized the rim size, excluded intervening airways, and constructed a nodule mask. The whole nodule mask was then split into subsolid voxel (Vsubs) and solid voxel (Vsol) components, defined using a solid density threshold of −188 Hounsfield units (HU). The percentage of solid density was then defined as

$$\%\ \text{Solid} = \text{Vsol}/(\text{Vsol} + \text{Vsubs})$$

Volumetric analyses were compared to data derived by analyzing a histogram of attenuation values within the nodule mask, using standard formulas to compute mean density (HU), standard deviation of HU (stdev), skewness, kurtosis, entropy, and the average attenuation of each of the four quartiles

TABLE 1. Quantitative imaging measurements of invasive adenocarcinoma (INV) and lepidic predominant lesions (LPL), a group that includes both lepidic predominant (LPA) and minimally invasive adenocarcinoma (MIA) ($P < .05$)

Measure	Mean INV	SD INV	Mean LPL	SD LPL	t	*P*
Volume (mm^3)	3558.0	3680.8	1663.5	2597.4	–2.380	.020
Size (mm)	8.2	3.0	5.9	2.8	–3.008	.004
Solid vol (mm^3)	1627.3	2352.6	219.1	416.8	–3.834	<.001
% Solid	35.4	20.2	9.0	8.4	–7.426	<.001
Skewness	0.352	0.584	1.350	0.757	5.308	<.001
Kurtosis	–0.419	0.839	2.938	5.977	2.552	.013
Entropy	6.516	0.279	5.896	0.462	–5.651	<.001
Mean HU	–315	114	–479	82	–6.567	<.001
Hu_Q1	–598	51	–645	17	–5.436	<.001
Hu_Q2	–419	136	–568	56	–6.206	<.001
Hu_Q3	–237	159	–459	105	–6.660	<.001
Hu_Q4	–10	134	–247	154	–6.017	<.001

HU, Hounsfield unit; INV, invasive adenocarcinoma; LPL, lepidic predominant lesions; SD, standard deviation.

(Hu_Q1–Hu_Q4) comprising the histogram. These data were analyzed using proprietary, in-house software (31).

Statistical Analyses

t-Test was used to compare differences between INV and LPL groups. A binomial logistic regression model was used to identify the best set of imaging features to distinguish INV from LPL nodules; initial variables in the model were nodule size and % solid, as previously reported (13). Each additional multivariate model included nodule size as an independent variable. Additional variables were tested for inclusion in the regression model, based on changes in chi-square statistic (32). If the change was significant at a $P = .10$ entry level, the variable was added to the model (ie, "forward conditional" logic). The model was then estimated through an iterative maximum likelihood algorithm. Varying probability cutoff values were tested to evaluate specificity and sensitivity, based on the premise that a false-negative error misclassifying an invasive lesion as benign presents greater harm than a false-positive error. Scatter plots were used to better understand if a variable provided a unique explanatory contribution, one that is not accounted for by variables already in the model, such as nodule size and % solid. A receiver operating characteristic (ROC) curve was constructed plotting the false-positive rate versus sensitivity. Each point on the ROC curve represents the false-positive rate and sensitivity at a different decision threshold. The area under the ROC curve (AUC) indicates the overall predictive performance of the multivariate model. Chi-square analysis was used to determine the goodness of fit. A *P* value <.05 was considered statistically significant. Statistical analysis was performed using SPSS Statistics 23 (IBM Corporation, Armonk, NY).

RESULTS

All quantitative imaging measurements significantly differentiated between INV ($n = 21$) and LPL ($n = 43$) groups (Table 1). This includes nodule size, 3D volumetric data such as total nodule volume, solid volume, and % solid, as well as all histogram features including skewness and entropy. There is also a significant difference between INV and LPL groups by overall mean nodule attenuation (HU) and attenuation among each of the four histogram quartiles. On multivariate analysis, logistic regression model M1, which was based on variables (1) size and (2) % solid, had overall accuracy of 85.9% (Table 2), with low sensitivity (61.9%) but very high specificity (97.7%) for differentiating LPL and INV. The odds ratio for % solid volume was 1.17. Thus, for each 1% increase in the solid component, we expect approximately 17% increased odds of a nodule being INV.

TABLE 2. Binomial regression models differentiating INV from LPL

Model	Model 1	Model 2
Independent variables	*Size* *%solid*	*Size* *Hu_Q3*
Chi-square	37.1	30.1
Log likelihood	43.9	50.9
Overall accuracy	85.9%	81.3%
P Value	<0.001	<0.001
Generalized R^2	0.440	0.375

INV, invasive adenocarcinoma; LPL, lepidic predominant lesions.

To avoid the use of a fixed density threshold of –188 HU to determine ground glass and solid components, an alternate multivariate logistic model that would not involve % solid was considered. This resulted in logistic regression model M2 (Table 2 and Fig 2), which is based on the independent variable size as well as average attenuation of the third quartile of the histogram (Hu_Q3). This model (M2) demonstrated an overall accuracy of 81.3%. The overall predictive performance indicated by AUC for M1 (based on % solid) is 0.897, with 95% confidence intervals (0.821–0.973). The AUC es-

TABLE 3. Prediction of invasive adenocarcinoma for two models at varying probability cutoffs

	Model M1				Model M2			
Cutoff	#FNeg	Sens	#Fpos	Spec	#Fneg	Sens	#Fpos	Spec
0.50	8	61.9%	1	97.7%	8	61.9%	4	90.7%
0.45	8	61.9%	2	95.3%	8	61.9%	4	90.7%
0.40	8	61.9%	6	86.0%	7	66.7%	6	86.0%
0.35	7	66.7%	9	79.1%	6	71.4%	7	83.7%
0.30	6	71.4%	9	79.1%	5	76.2%	11	74.4%
0.25*	4	81.0%	10	76.7%	4	81.0%	12	72.1%
0.20	2	90.5%	15	65.1%	2	90.5%	15	65.1%
0.15	1	95.2%	16	62.8%	2	90.5%	16	62.8%

#F neg, number of false-negative cases; #F pos, number of false-positive cases; Sens, sensitivity; Spec, specificity.
* The cutoff of 0.25 provides an optimal balance of sensitivity and specificity.

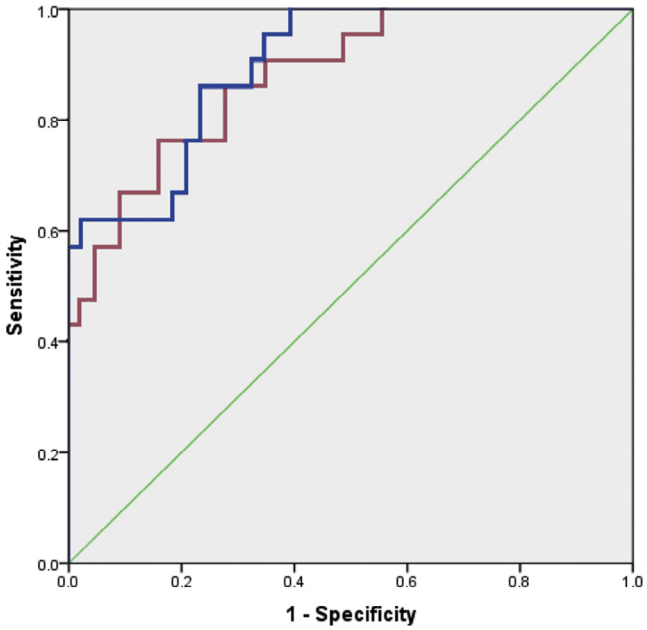

Figure 2. Receiver operating characteristic (ROC) curves for prediction of invasive adenocarcinoma (INV) based on two models. Blue line: model (M1) based on nodule size and % solid. Red line: model (M2) based on nodule size and third quartile of nodule attenuation (Hu_Q3). The green line indicates an uninformative (worthless) prediction. Note similar areas under both ROC curves for both M1 and M2 models. (Color version of figure is available online.)

timated for M2, based on histogram data, has a similar value of 0.877 and 95% confidence intervals (0.790–0.964).

In both multivariate logistic models, varying the probability cutoff alters diagnostic sensitivity (Table 3). The cutoff value of 0.25 provides a clinically useful sensitivity level of 81% for both M1 and M2 models. Figure 2 shows the resulting balance between sensitivity and specificity.

In spite of highly significant discrimination between INV and LPL based on numerous quantitative CT measurements, only % solid (M1) and Hu_Q3 (M2) qualified as independent contributors using *forward conditional* logic. Although it might have been anticipated that Hu_Q4 would show the best correlation with solid composition and therefore presumed invasiveness of nodules, our data showed a large variability of Hu_Q4 data, with pooled standard deviation of approximately 144 HU compared to Hu_Q3, resulting in preferential selection of Hu_Q3. Other quantitative CT features were unable to provide additional discrimination in multivariate analysis; the explanation for this lack of added utility of other measurements is their mutual correlation. Figure 3 illustrates similar scatter plots involving Hu_Q3 and the histogram measurement of entropy, for example.

DISCUSSION

Despite formal inclusion of LPA as an invasive form of lung adenocarcinoma, previous pathologic reports have documented that lepidic predominant lesions (AIS, MIA, and LPA) have clearly improved prognosis compared to more invasive adenocarcinomas (15–19). This includes reports of improved DFS in a combined group of patients with LPL, compared to groups of other invasive subtypes (17,33).

To date, and in marked distinction to pathology reports, nearly all imaging literature has emphasized the distinction of pre- and minimally invasive lesions (AIS and MIA) from all invasive adenocarcinomas (22,25,34), ignoring the possibility of radiologic differentiation among the various forms of invasive disease, despite wide variation in the prognosis of these lesions. In one unique study involving only pure ground glass nodules, 92 of 191 lesions proved to be invasive carcinoma; this group of invasive lesions included 49 lepidic predominant, 40 acinar predominant, and 3 papillary predominant specimens (35). Multivariate logistic regression analysis identified the 75th percentile CT attenuation ($P = .004$) and entropy ($P < .01$) as independent predictors of invasive carcinoma with an AUC of 0.78. Altogether, the disease-free interval for invasive carcinomas was 97.7% (90 of 92 patients), with recurrence only in papillary predominant cases. Despite these findings, these authors note imaging variables such as visual assessment, volume, density, mass, skewness, and kurtosis failed to reach clinical significance when corrected for multivariate analysis in differentiating this combined cohort of invasive lesions from minimally and preinvasive disease (35).

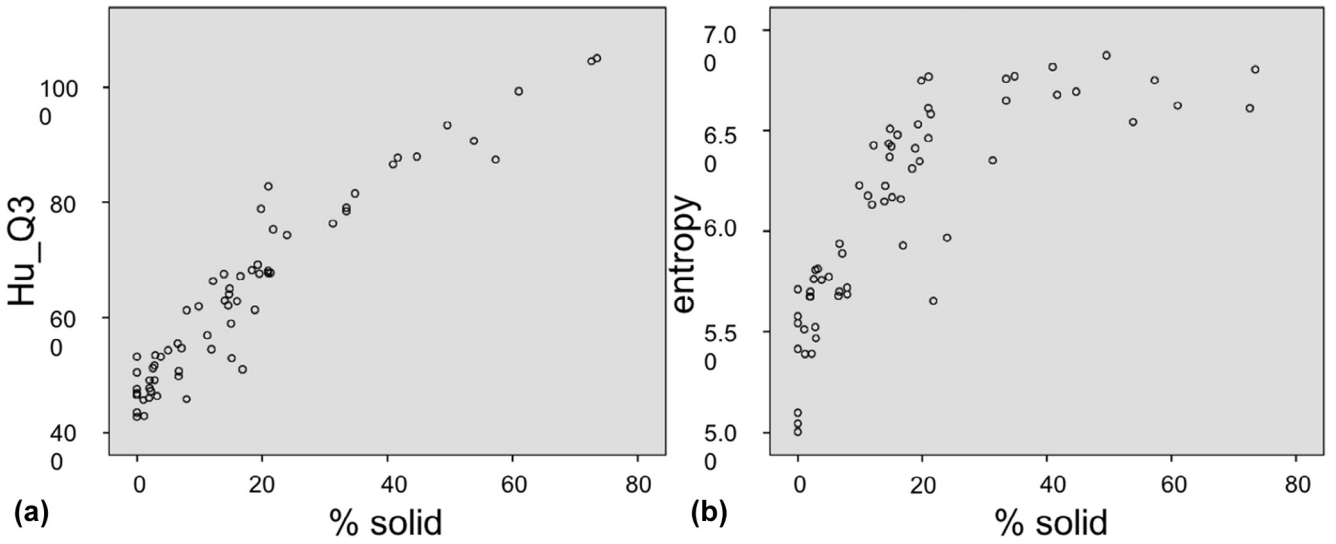

Figure 3. There was a very high correlation between % solid and two different histogram measures. **(a)** Average attenuation of the third quartile (Hu_Q3), Pearson R = 0.949, $P < .001$. **(b)** Entropy, Pearson R = 0.767, $P < .001$.

Our study builds on prior literature and documents that CT-based 3D volumetric density and histogram features are significantly different between lepidic predominant pulmonary lesions and more invasive adenocarcinoma subtypes. Univariate analysis shows that a broad range of quantitative CT findings have statistical significance for differentiating LPL from INV lesions, including nodule size, 3D volumetric density measurements of total nodule volume, solid nodule volume, and % of solid volume, as well as all selected histogram measurements including mean nodule attenuation overall and mean attenuation of each of the four histogram quartiles. More importantly, multivariate regression models are also able to differentiate the two groups independent of nodule size, with similar accuracy of up to nearly 86%. Using binomial regression models for differentiating LPL from INV, a combination of variables size and % solid (model 1, using 3D volumetric density data) has comparable but slightly higher accuracy than a combination of size and Hu_Q3 (model 2, using histogram data), with accuracy of 85.9% and 81.3%, respectively. Comparison of ROC curves predicting more invasive disease also documents similarity of these two models. Although slightly less accurate, M2 histogram-based data show that differentiation between LPL and INV groups is possible without dependence on a CT density threshold to separate solid and nonsolid voxels.

Our study advances prior work regarding the ability to differentiate lesions on the adenocarcinoma spectrum based on quantitative CT volumetric assessment. Using the same semiautomated computer program, 41 lesions were previously evaluated with quantitative CT regarding total nodule volume and mass, solid nodule volume and mass, and % solid volume and mass. This study used three specimen groups: combined pre- and minimally invasive specimens, LPA, and INV subtypes. There was a significant difference in % solid volume between LPA and INV lesions (14.5% versus 35.4%, $P = .002$). Accuracy of a logistic regression model incorporating total nodule volume and % solid volume was 73.2% (13).

Although preliminary, our current work implies a potential clinical benefit in applying IASLC/ATS/ERS classification to group all LPL, including LPA, apart from more invasive lung adenocarcinoma subtypes. These conclusions include potential management implications, which could be further investigated with prospective, longitudinal evaluation, specifically regarding a more conservative approach to patients with LPL, in the appropriate clinical setting such as advanced comorbid disease or the presence of multiple lesions.

Although our findings suggest a potential role for detailed subtyping of undifferentiated invasive adenocarcinoma by quantitative CT evaluation of lung nodules, major limitations remain. These include determining which volumetric measurements are most clinically important, as well as the variability among reported methods of lung nodule segmentation (20,24,36–44). Regarding histogram analysis, various segmentation algorithms include manual versus semiautomated and two-dimensional versus 3D segmentation, and there is marked variation regarding which histogram features prove most valuable (22,24–27,35). Few studies have attempted to correlate histogram analyses with the current IASLC/ATS/ERS classification of peripheral adenocarcinomas (26,29). Furthermore, few reports attempt to directly correlate advanced 3D volumetric evaluation with histogram analysis to determine which method of evaluation is more useful; our results demonstrate similar accuracy between multivariate analyses based on 3D volumetric data and histogram data. Although these findings strengthen the position of quantitative CT histogram analysis as a credible method of evaluation, this also demonstrates slightly lower accuracy compared to volumetric data. Nodule morphology plays a role in this evolving field, with some studies including only pure ground glass nodules and others evaluating part-solid or predominantly solid lesions (22,25,35).

Variation also arises from the histopathology assessed, with some studies including all cases of non–small cell lung cancer and others evaluating only peripheral adenocarcinomas (22,25,26,35). Few reports emphasize potential prognostic implications and/or correlation with surgical staging (26,27).

Limitations specific to this study include a small sample size of 43 specimens. Three available specimens of AIS were excluded from this study because of their small number; this also likely reflects the rarity of surgical resection of these preinvasive lesions. Although this study includes first-order texture analysis, second-order analysis is considered more advanced because of its ability to provide information regarding spatial relationships and correlations between voxels (45). However, this technique remains less standardized and requires more advanced technology, resulting in our decision to currently focus on first-order texture analysis.

REFERENCES

1. Noguchi M, Morikawa A, Kawasaki M, et al. Small adenocarcinoma of the lung. Histologic characteristics and prognosis. Cancer 1995; 75:2844–2852.
2. Jiang B, Takashima S, Miyake C, et al. Thin-section CT findings in peripheral lung cancer of 3 cm or smaller: are there any characteristic features for predicting tumor histology or do they depend only on tumor size? Acta Radiol 2014; 55:302–308.
3. Honda T, Kondo T, Murakami S, et al. Radiographic and pathological analysis of small lung adenocarcinoma using the new IASLC classification. Clin Radiol 2013; 68:e21–e26.
4. Kim HY, Shim YM, Lee KS, et al. Persistent pulmonary nodular ground-glass opacity at thin-section CT: histopathologic comparisons. Radiology 2007; 245:267–275.
5. Lim HJ, Ahn S, Lee KS, et al. Persistent pure ground-glass opacity lung nodules >/= 10 mm in diameter at CT scan: histopathologic comparisons and prognostic implications. Chest 2013; 144:1291–1299.
6. Zhang Y, Qiang JW, Ye JD, et al. High resolution CT in differentiating minimally invasive component in early lung adenocarcinoma. Lung Cancer 2014; 84:236–241.
7. Takahashi M, Shigematsu Y, Ohta M, et al. Tumor invasiveness as defined by the newly proposed IASLC/ATS/ERS classification has prognostic significance for pathologic stage IA lung adenocarcinoma and can be predicted by radiologic parameters. J Thorac Cardiovasc Surg 2014; 147:54–59.
8. Lee SM, Park CM, Goo JM, et al. Invasive pulmonary adenocarcinomas versus preinvasive lesions appearing as ground-glass nodules: differentiation by using CT features. Radiology 2013; 268:265–273.
9. Lee KH, Goo JM, Park SJ, et al. Correlation between the size of the solid component on thin-section CT and the invasive component on pathology in small lung adenocarcinomas manifesting as ground-glass nodules. J Thorac Oncol 2014; 9:74–82.
10. Van Riel S, Sanchez CL, Bankier AA, et al. Observer variability for classification of pulmonary nodules on low-dose CT images and its effect on nodule management. Radiology 2015; 277:863–871.
11. Heidinger BH, Anderson KR, Nemec U, et al. Lung adenocarcinoma manifesting as pure ground-glass nodules: correlating CT size, volume, density, and roundness with histopathologic invasion and size. J Thorac Oncol 2017; 12:1288–1298.
12. Zhou QJ, Zheng ZC, Zhu YQ, et al. Tumor invasiveness defined by IASLC/ATS/ERS classification of ground-glass nodules can be predicted by quantitative CT parameters. J Thorac Oncol 2017; 9:1190–1200.
13. Ko JP, Suh J, Ibidapo O, et al. Lung adenocarcinoma: correlation of quantitative CT findings with pathologic findings. Radiology 2016; 280:931–939.
14. Travis WD, Brambilla E, Noguchi M, et al. International Association for the Study of Lung Cancer/American Thoracic Society/European Respiratory Society International multidisciplinary classification of lung adenocarcinoma. J Thorac Oncol 2011; 6:244–285.
15. Kadota K, Villena-Vargas J, Yoshizawa A, et al. Prognostic significance of adenocarcinoma in situ, minimally invasive adenocarcinoma, and nonmucinous lepidic predominant invasive adenocarcinoma of the lung in patients with stage 1 disease. Am J Surg Pathol 2014; 38:448–460.
16. Yanagawa N, Shiono S, Abiko M, et al. The correlation of the International Association for the Study of Lung Cancer (IASLC)/American Thoracic Society (ATS)/European Respiratory Society (ERS) classification with prognosis and EFGR mutation in lung adenocarcinoma. Ann Thorac Surg 2014; 98:453–458.
17. Yoshizawa A, Motoi N, Riely G, et al. Impact of proposed IASLC/ATS/ERS classification of lung adenocarcinoma: prognostic subgroups and implications for further revision of staging based on analysis of 514 stage 1 cases. Mod Pathol 2011; 24:653–664.
18. Yoshizawa A, Sumiyoshi S, Sonobe M, et al. Validation of the IASLC/ATS/ERS lung adenocarcinoma classification for prognosis and association with EGFR and KRAS mutations. Analysis of 440 Japanese patients. J Thorac Oncol 2013; 8:52–61.
19. Russell PA, Wainer Z, Wright GM, et al. Does lung adenocarcinoma subtype predict patient survival? J Thorac Oncol 2011; 6:1496–1504.
20. Yanagawa M, Tanaka Y, Leung AN, et al. Prognostic importance of volumetric measurements in stage 1 lung adenocarcinoma. Radiology 2014; 272:557–567.
21. Yanagawa N, Shiono S, Abiko M, et al. New IASLC/ATS/ERS classification and invasive tumor size are predictive of disease recurrence in stage I lung adenocarcinoma. J Thorac Oncol 2013; 8:612–618.
22. Chae H-D, Park CM, Park SJ, et al. Computerized texture analysis of persistent part-solid ground-glass nodules: differentiation of preinvasive lesions from invasive pulmonary adenocarcinomas. Radiology 2014; 273:285–293.
23. Davnall F, Yip CSP, Ljungqvist G, et al. Assessment of tumor heterogeneity: an emerging imaging tool for clinical practice. Insights Imaging 2012; 3:573–589.
24. Ikeda K, Awai K, Mori T, et al. Differential diagnosis of ground-glass opacity nodules. CT number analysis by three-dimensional computerized quantification. Chest 2007; 132:984–990.
25. Kamiya A, Murrryama S, Kamiya H, et al. Kurtosis and skewness assessments of solid lung nodule density histograms: differentiating malignant from benign nodules. Jpn J Radiol 2014; 32:14–21.
26. Kawata Y, Niki N, Ohmatsu H, et al. Quantitative classification based on CT histogram analysis of non-small cell lung cancer: correlation with histopathological characteristics and recurrence-free survival. Med Phys 2012; 39:988–1000.
27. Lee SH, Lee SM, Goo JM, et al. Usefulness of texture analysis in differentiating transient from persistent part-solid nodules (PSNs): a retrospective study. PLoS ONE 2014; 9:e85167.
28. Nomori H, Ohtsuka T, Naruke T, et al. Differentiating between atypical adenomatous hyperplasia and bronchoalveolar carcinoma using the computed tomography number histogram. Ann Thorac Surg 2003; 76:867–871.
29. Son JY, Lee HY, Kim J, et al. Quantitative CT analysis of pulmonary ground-glass opacity nodules for distinguishing invasive adenocarcinoma from non-invasive or minimally invasive adenocarcinoma: the added value of using iodine mapping. Eur Radiol 2016; 26:43–54.
30. Ko JP, Berman EJ, Kaur M, et al. Pulmonary nodules: growth rate assessment in patients using serial CT and three-dimensional volumetry. Radiology 2013; 262:662–671.
31. Lestrel PE. Biological Shape Analysis. 2011;324.
32. Bursac Z, Gauss CH, Williams DK, et al. Purposeful selection of variables in logistic regression. Source Code Biol Med 2008; 16:17.
33. Warth A, Muley T, Meister M, et al. The novel histologic International Association for the Study of Lung Cancer/American Thoracic Society/European Respiratory Society classification system of lung adenocarcinoma is a stage-independent predictor of survival. J Clin Oncol 2012; 30:1438–1446.
34. Hwang I-P, Park CM, Park SJ, et al. Persistent pure groundglass nodules larger than 5 mm: Differentiation of invasive pulmonary adenocarcinomas from preinvasive lesions or minimally invasive adenocarcinomas using texture analysis. Invest Radiol 2015; 50:798–804.
35. Son JY, Lee HY, Kim J-H, et al. Quantitative CT analysis of pulmonary ground-glass opacity nodules for the distinction of invasive adenocarcinoma from pre-invasive or minimally invasive adenocarcinoma. PLoS ONE 2014; 9:e104066.

36. de Hoop B, Gietema H, van de Vorst S, et al. Pulmonary ground-glass nodules: increase in mass as an early indicator of growth. Radiology 2010; 255:199–206.
37. Kim H, Park CM, Woo S, et al. Pure and part-solid pulmonary ground-glass nodules: measurement variability of volume and mass in nodules with a solid portion less than or equal to 5 mm. Radiology 2013; 269:585–593.
38. Oda S, Awai K, Murao K, et al. Volume-doubling time of pulmonary nodules with ground glass opacity at multidetector CT: assessment with computer-aided three-dimensional volumetry. Acad Radiol 2011; 18:63–69.
39. Oda S, Awai K, Murao K, et al. Computer-aided volumetry of pulmonary nodules exhibiting ground-glass opacity at MDCT. AJR Am J Roentgenol 2010; 194:398–406.
40. Park CM, Goo JM, Lee HJ, et al. Persistent pure ground-glass nodules in the lung: interscan variability of semiautomated volume and attenuation measurements. AJR Am J Roentgenol 2010; 195:1315.
41. Sumikawa H, Johkoh T, Nagareda T, et al. Pulmonary nodules with ground-glass attenuation on thin-section CT: quantification by three-dimensional image analyzing method. Eur J Radiol 2008; 65:104–111.
42. Van Klaveren RJ, Oudkerk M, Prokop M, et al. Management of lung nodules detected by volume CT scanning. N Engl J Med 2009; 361:2221–2229.
43. Yanagawa M, Kuriyama K, Kunitomi Y, et al. One-dimensional quantitative evaluation of peripheral lung adenocarcinoma with or without ground-glass opacity on thin-section CT images using profile curves. Br J Radiol 2009; 82:532–540.
44. Yanagawa M, Tanaka Y, Kusumoto M, et al. Automated assessment of malignant degree of small peripheral adenocarcinomas using volumetric CT data: correlation with pathologic prognostic factors. Lung Cancer 2010; 70:286–294.
45. Nailon WH. Texture analysis methods for medical image characterisation. In: Mao Y, ed. Biomedical imaging. 2010; 75–100.